geographies

MDPI

Article

Assessing the Efficiency of Fully Two-Dimensional Hydraulic HEC-RAS Models in Rivers of Cyprus

Georgia Siakara, Nikolaos Gourgouletis * and Evangelos Baltas *

Department of Water Resources & Environmental Engineering, School of Civil Engineering, National Technical University of Athens, Str. Iroon Politexniou 9, 157 80 Zografou, Greece
* Correspondence: gourgouletisnik@mail.ntua.gr (N.G.); baltas@central.ntua.gr (E.B.)

Abstract: Floods are among the most widespread and recurrent natural disasters globally. In the European region, climate change leads to an increase in the incidence and intensity of flooding. For effective management of the phenomenon, the European Union instituted Directive 2007/60/EC for the assessment and management of flood risks in order to reduce the negative consequences of flooding on human health, economic activities, the environment, and cultural heritage. Cyprus, as a member of the European Union, had to comply with the provisions of the directive. Within the second implementation of the directive, combined 1D/2D hydraulic models were conducted. These data served as a benchmark for the present research, in which the differences in the inundated area, depths, and simulation time are investigated using a full 2D hydraulic simulation. The present research examines two Areas of Potentially Significant Flood Risk, one in an urban and one in a rural area. Overall, the proposed 2D methodology was found to represent inundated areas to a good extent with almost zero deviation in comparison to the 1D/2D method. This study demonstrated the adequacy of the 2D hydraulic simulation method, which offers greater flexibility in modeling a variety of hydraulic scenarios, enabling planning and flood risk management that is vital for protecting communities, infrastructure and the environment from the devastating impacts of floods.

Keywords: hydraulic simulation; floods; HEC-RAS; 2-D analysis; Cyprus

check for updates

Citation: Siakara, G.; Gourgouletis, N.; Baltas, E. Assessing the Efficiency of Fully Two-Dimensional Hydraulic HEC-RAS Models in Rivers of Cyprus. *Geographies* **2024**, *4*, 513–536. https://doi.org/10.3390/geographies4030028

Academic Editor: Xu Chen

Received: 24 May 2024
Revised: 26 July 2024
Accepted: 31 July 2024
Published: 5 August 2024

Copyright: © 2024 by the authors. Licensee MDPI, Basel, Switzerland. This article is an open access article distributed under the terms and conditions of the Creative Commons Attribution (CC BY) license (https://creativecommons.org/licenses/by/4.0/).

1. Introduction

Flooding is a recurrent natural phenomenon characterized by the temporary inundation of land not typically submerged by water [1]. Floods rank among the most recurrent and widespread natural disasters globally [2,3], constituting 44% of all disaster occurrences between 2000 and 2019, resulting in the loss of 1.23 million lives, affecting 4.2 billion people and leading to economic losses estimated at USD 2.97 trillion worldwide [4]. In the Mediterranean region, a cyclone named 'Medicane Daniel' caused floods in Greece and neighboring countries, resulting in economic losses reaching USD 17 billion in Europe [5].

Southern Europe and the Mediterranean region are at high vulnerability to climate change impacts [5–7], suffering from temperature increases, considerable reductions in rainfall and water runoff, and extreme events (e.g., flash floods and heatwaves) [5,8,9]. These changes manifest in various forms, including increased intensity and frequency of rainfall events, leading to heightened flood risk [10]. Moreover, sea-level rise exacerbates coastal flooding, posing additional challenges to vulnerable coastal communities [11]. However, effective adaptation strategies require a comprehensive understanding of the complex interactions between climate change, land use patterns, and hydrological processes [7,8,12]. In the hydraulic simulation process, another critical parameter is the selection of the appropriate time series analysis method, which should be based on the geomorphological characteristics of the area under consideration [13,14].

Especially, Cyprus, an island located in the eastern Mediterranean basin, experiences a temperate climate with scorching, arid summers, and according to the Köppen–Geiger

classification system, a portion of the island is deemed hot and arid [15,16]. A study spanning up to the year 2030 indicates that the annual cost of water scarcity in the domestic and industrial sectors could reach up to EUR 88 million. From this amount, EUR 16–32 million would constitute additional costs due to reduced water availability attributed to climate change [17].

To manage and monitor floods within urban areas, the European Commission implemented Flood Directive 2007/60/EC. This framework primarily aims to mitigate the adverse impacts of floods on the environment, human health, cultural heritage, and economic activities closely tied to society [12,18]. Member states of the European Union were required to establish River Basin Flood Risk Management Plans, which identify vulnerable areas while considering long-term developments and future flood occurrences. The primary objective of flood risk assessment at the national level is the creation of flood hazard maps [19,20]. These maps depict flood extent, depth, flow speed, and probability. Furthermore, flood risk maps evaluate potential adverse consequences for the economic activity of the region and for potentially affected residents [1].

Cyprus, as a member of the European Union, has achieved full compliance with the provisions of Directive 2007/60. Moreover, Cyprus harmonized with the provisions of the directive by transposing them into Cypriot law [21]. Specifically, it enacted the laws of 2010 and 2012 [22]. The legislation enacted in July 2010 designates the Tax Department as the Competent Authority for the implementation of the directive and the Ministry of Interior as the Coordinating Authority. Specifically, Cyprus has already completed the second implementation cycle of the directive, which is in force until 2027 [22].

Flood warning and forecasting systems play a major role in flood risk management; specifically, the evaluation of flood hazard achieved by inundation mapping and identification of flood risk regions [23–25]. Flood inundation modeling plays a crucial role in generating spatial distribution data pertaining to inundation patterns, including water depth and flow velocity. This information can provide insights into the severity of the hazard, potential risks to public safety, and potential financial implications [2,12,26–29].

Appropriate and effective tools for flood inundation modeling and mapping assist with flood risk assessment. Primarily, these requirements have been evaluated through the utilization of one-dimensional (1D) and two-dimensional (2D) hydraulic models (e.g., [30,31]. Hydraulic simulation, through advanced modeling techniques, offers a valuable tool for assessing and mitigating flood risks, particularly in the context of emergency preparedness. The integration of hydraulic simulation into emergency management frameworks enables authorities to anticipate and respond effectively to flood events, thus minimizing the potential impact on communities and infrastructure. By simulating various scenarios, policymakers can identify vulnerable areas, evaluate evacuation routes, and develop targeted response strategies [27–29]. Moreover, hydraulic simulation facilitates the testing and optimization of flood protection measures, enhancing the resilience of communities to future disasters.

This research presents a practical framework for mapping flood inundation in ungauged urban areas, tailored for the context of the EU Floods Directive's second implementation in Cyprus. The framework's efficacy is demonstrated in Larnaca and Nicosia, regions prone to frequent flooding from intense storms. The comparison between different hydraulic simulation methods enhances our ability to accurately estimate and delineate flood-prone areas, assess the uncertainty inherent in flood mapping, offer guidance to flood management professionals, and inform the development of protective measures and policies safeguarding human life, property, and economic assets.

2. Materials and Methods

2.1. Study Areas

This research's study area consists of two Areas of Potentially Significant Flood Risk (APSFR), which are specified from the second implementation of the Floods Directive

in Cyprus. The abovementioned areas are two river systems, Vasilikos—Asgatas and Vyzakotos—Kalogeros, located in the region of Cyprus (Figure 1).

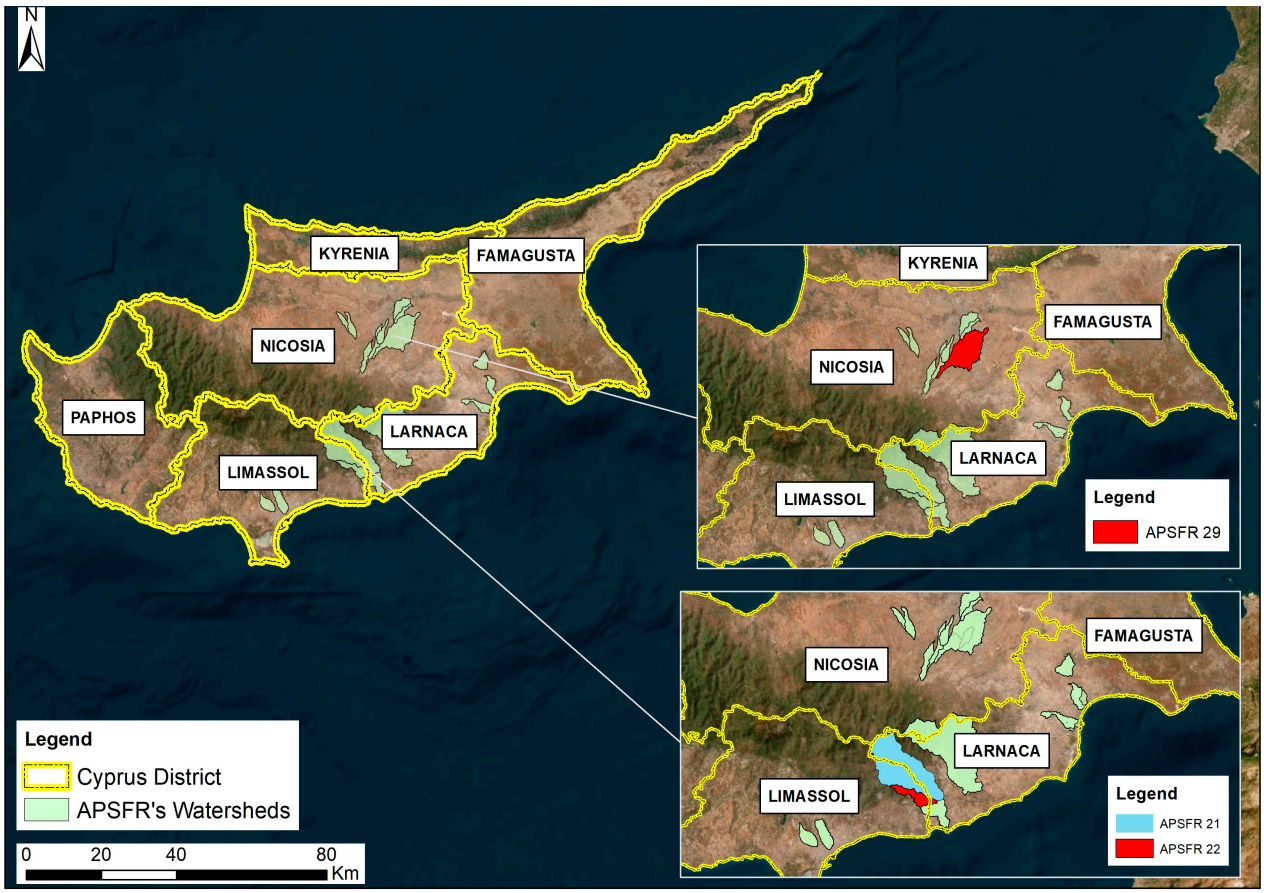

Figure 1. Study watersheds based on the second implementation of Directive 2007/60.

Vasilikos—Asgatas watershed with codename APSFR 21–22 belongs to the districts of Larnaca and Limassol; the area of each part is 114.9 km^2 and 16.82 km^2. Vasilikos River has a length of 2.51 km and a longitudinal slope of 1.4% with southeast movement. Asgatas River junctions Vasilikos River from the west, upstream of the Kalavasos settlement. The river, located in APSFR 22, is characterized by a length of 0.43 km, a 1.9% slope, and intensive vegetation [22].

The predominant soil in the catchment area of APSFR 21–22 is characterized by a high potential for surface runoff, mainly in the upstream part. The soils are shallow (<50 cm), gravelly, or clayey over impermeable rock. A characteristic feature of these soils is the unfavorable saturation conditions in the event of flooding events due to the composition of the subsoil, which does not facilitate subsidence. Hydrographic networks are characterized as dense and dendritic with numerous streams and brooks forming small gorges moving through deep valleys [21,32]. Primary flooding mechanisms include the natural overflow of the river and the obstruction of bridges by debris. Additionally, the overflow of the Kalavasos Dam, situated upstream of APSFR 21, may contribute to flooding under extreme return period events. Also, significant flooding problems have been reported at the confluence of APSFR 21 and APSFR 22. Locations reported for flooding incidents are shown in the relevant Figure in Section 3.4.1.

The second river system, Vyzakotos-Kalogeros, with codename APSFR 29, located in the district of Limassol, occupies a catchment area of 58.99 km^2, a length of 10.85 km, and a 0.8% slope [22].

The catchment area of APSFR 29 consists mainly of residential, industrial, and commercial land. The geological composition of the soils in the area is mainly clayey and loamy. The

soils are mostly of moderate depth (50–100 cm) with some areas of shallow (<50 cm) and deep (>100 cm) soils. From a geological point of view, the basin has no stable permeability. In the upstream part, it is characterized as low to relatively low, while in the downstream part it is characterized as medium. The hydrographic network is characterized as dendritic with a high density of streams and water sources [22]. According to Cypriot authorities, flooding problems in the study area occur during normal return periods. Additionally, a flood-prone river section is located to the southeast of the University of Cyprus sports facilities (Location Number 1). Locations where flooding incidents have been reported are presented in the relevant Figure in Section 3.4.2.

2.2. Data Used

For the purposes of this research, the Cyprus Water Development Department provided combined 1D/2D hydraulic simulation models that have been developed for the requirements of the second implementation cycle of Directive 2007/60. Preliminary flood assessment identified 19 additional APSFR (38 in total, including 19 APSFR existing from the first implementation) [22]. Hydraulic simulation for those areas was carried out using HEC-RAS (Hydrologic Engineering Center—River Analysis System) software in version 6.3.1, in combined 1D/2D simulation. This software was also used in the first implementation cycle.

It is noted that there is not sufficient in situ data regarding flood discharges. Thus, it is not feasible to validate the results of both the 1D/2D and the 2D models with actual flood events. Therefore, as also noted in Section 1, the scope of the present research consists of the comparison between different hydraulic simulation methods.

2.2.1. Manning and Land Uses

The coefficient of roughness or Manning number expresses the losses due to friction along the water flow (Robert Manning, 1889) through the following Equation (1):

$$Q = \left(\frac{1}{n}\right) A R^{\frac{2}{3}} \sqrt{S} \quad (1)$$

where Q is the flow rate (m^3/s), A is the surface (m^2), n is the Manning number, R is hydraulic radius (m), and S is the flow gradient (m/m).

The values of the Manning number in two-dimensional analysis depend on the respective land use and are equal to or higher than the values of the one-dimensional analysis in order to represent the higher energy losses of the flow outside the main channel. Thus, Manning coefficients were determined based on land uses [22] (for detail, see Table 1):

Table 1. Manning values have been used in hydraulic simulation.

Land Use	Manning Coefficient
Sclerophyllous vegetation	0.067
Complex cultivation with scattered crops	0.050
Discontinuous urban fabric	0.066
Roads	0.015
Discontinuous, low density urban fabric	0.088
Discontinuous, very low-density urban fabric	0.100
Non-irrigated arable land	0.070
Isolated structures	0.100
Industrial, public, commercial, military, and private uses	0.050
Agricultural land with natural vegetation	0.060

Manning values are inserted in hydraulic models as a shapefile from HEC-RAS Mapper, and same-valued polygons are created, where each of which represents a specific Manning value. Manning values assumed for the purposes of this study are presented in the following Figure 2 for APSFR 21–22 and 29, respectively.

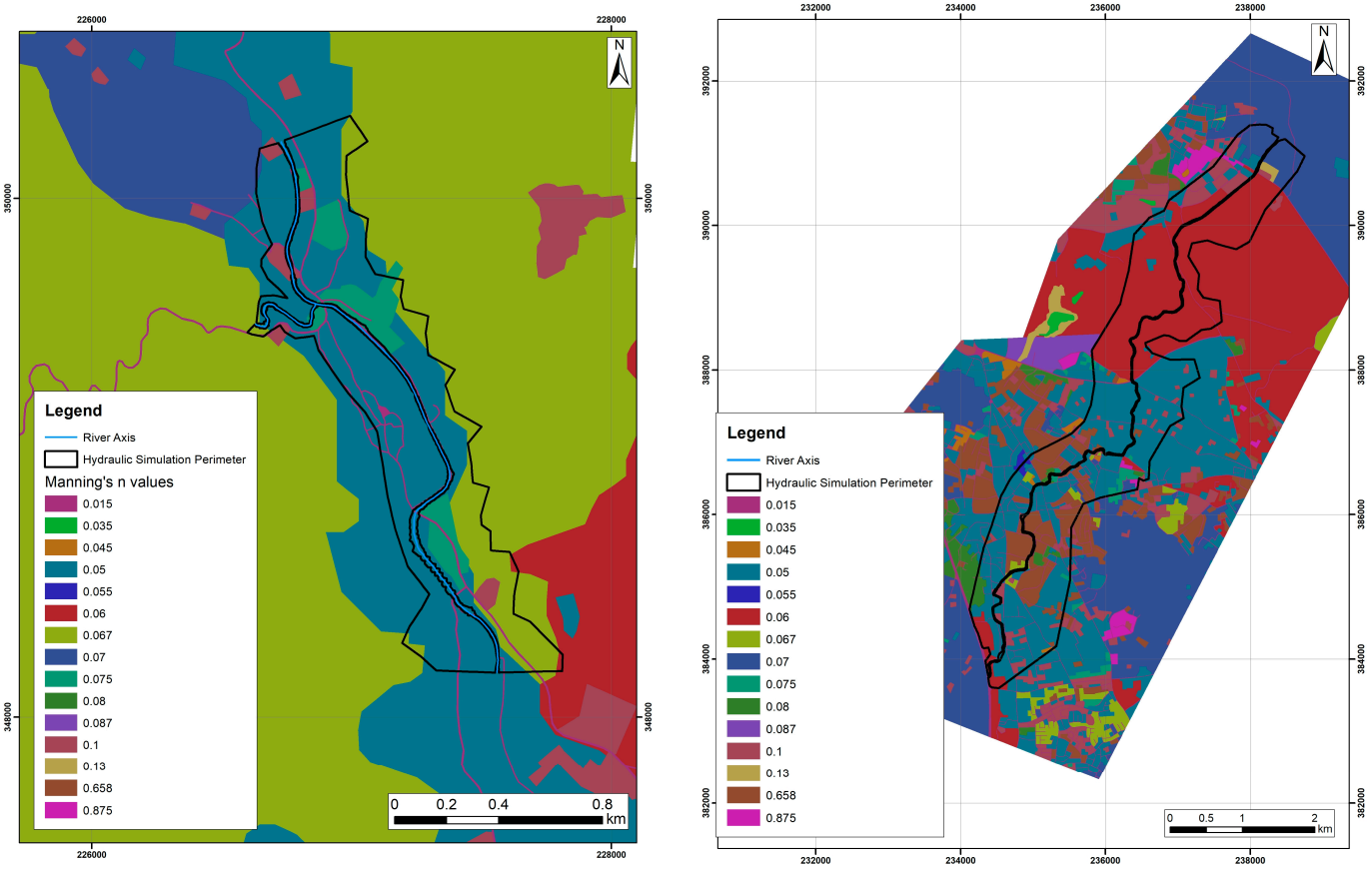

(**a**) (**b**)

Figure 2. (**a**) Manning's n values for APSFR 21-22, (**b**) Manning's n values for APSFR 29.

2.2.2. DEM

The Digital Elevation or Terrain Model is the representation of the earth's surface, referred to as geomorphometry [33,34]. The digital terrain model depicts the ground elevations in very high definition of 1 m × 1 m and is provided by the Cyprus Cadastre. In general, it is a high-resolution model as it represents with sufficient accuracy the terrain topography in the examined area [22].

2.2.3. Structures

By accurately modeling the interaction between water flow and structures such as bridges, culverts, and weirs, hydraulic simulations provide critical insights into their performance and resilience under various flow conditions. This allows engineers to predict potential issues, such as scour, sediment deposition, and structural failure, enabling proactive design adjustments, and maintenance planning. Furthermore, hydraulic simulations facilitate the optimization of structure placement and dimensions, ensuring minimal environmental impact and improved safety.

As for the hydraulic structures along the main river, there are 11 and 21 in each APSFR 21–22 and APSFR 29, respectively.

2.2.4. Hydrological Data

Hydrological data have been received from the Water Development Department of Cyprus and imported in hydraulic models as hydrographs. Hydrographs, representing the flow rate of water over time at a specific location, are introduced into HEC-RAS to simulate unsteady flow conditions. This is accomplished by defining boundary conditions at the model's inflow and outflow points. Hydrographs are being imported through the Boundary Conditions editor, selecting the appropriate river reach and cross-section locations. The hydrographs can be specified either as a time series of flow rates or water surface elevations, depending on the available data and the specific requirements of the simulation. The examined flood return periods are based on three hydrological scenarios: T = 20 years, 100 years, and 500 years. The abovementioned hydrological scenarios derive from the second FRMP of Cyprus and the corresponding hydrographs used for the purposes of the present research are identical to those applied to the 1D/2D FRMP hydraulic simulation.

2.3. Methodology

For the hydraulic simulation, the free software HEC-RAS version 6.3.1 developed by the U.S. Army Corps of Engineers (U.S.A.C.E.) was used. It is a complete software system ideal for interactive use with a wide range of features and users. The software performs calculations under permanent and non-permanent flow conditions and enables simulation of water level and sediment transport and deposition. It consists of a graphical user interface and has the ability to store, manage, and edit input and output data.

For the application of 2D modelling, the equations of continuity (mathematical expression of the mass conservation principle) and quantity of motion (mathematical expression of the conservation of momentum) are used. The Navier–Stokes equations describe the motion of fluids in three dimensions. Their integration yields equations suitable for shallow water.

To apply the equations to a flood risk study in two dimensions, appropriate considerations are made for shallow water (Shallow Water Equations). The assumptions made for the application of the Equations (2)–(4) are presented below:

- Preservation of mass:

$$\frac{\partial H}{\partial t} + \frac{\partial (hu)}{\partial x} + \frac{\partial (hv)}{\partial y} + q = 0 \tag{2}$$

where $H(x,y,t)$ is the water level (m), t is time, u,v are the depth, and q is the water flowrate (m^3/s).

- Conservation of Momentum:

  Momentum in x-direction:

$$\frac{\partial u}{\partial t} + u\frac{\partial u}{\partial t} + \frac{\partial u}{\partial y} = -g\frac{\partial H}{\partial x} + vt\left(\frac{\partial^2 u}{\partial x^2} + \frac{\partial^2 u}{\partial y^2}\right) - c_f + fv \tag{3}$$

  Momentum in y-direction:

$$\frac{\partial v}{\partial t} + u\frac{\partial v}{\partial t} + v\frac{\partial u}{\partial y} = -g\frac{\partial H}{\partial y} + vt\left(\frac{\partial^2 v}{\partial x^2} + \frac{\partial^2 v}{\partial y^2}\right) - c_f + fu \tag{4}$$

where u and v are the average velocities in the x, y direction (m/s), g is gravitational acceleration (m/s^2), c_f is the coefficient of the friction of the bottom (s^{-1}), and f (s^{-1}) is the Coriolis parameter

Under certain circumstances, in shallow water flow, the Coriolis parameter, the transport and local acceleration, and the viscosity are not taken into account. The equations of motion, in this case, are reduced to a two-dimensional form of the Diffusion Wave Approximation equations. Combining this equation with the mass conservation princi-

pal equation results in the Diffusion Wave Approximation of the Shallow Water (DSW) Equations (5) and (6) are presented below:

$$-g\frac{\partial H}{\partial x} = c_f u \tag{5}$$

$$-g\frac{\partial H}{\partial y} = c_f v \tag{6}$$

To decrease computational time and avoid numerical instabilities, the HEC-RAS 2D unsteady flow Saint-Venant equations (shallow water equations) are frequently simplified with the diffusive wave approximation. However, these simplifications are only appropriate under specific flow conditions. For rivers affected by tides, it is recommended to use the complete momentum equations [22].

For the arrangement of the 2-D hydraulic models, the following steps were followed:

1. Creating the Project.
2. Import the background from Ras Mapper as Terrain.
3. Creation of the geometry performed by Ras Mapper.
4. Drawing of the main riverbed is captured as Breakline and represents the flow axis of the stream under study.
5. Design of the perimeter is carried out through the 2D Flow Areas -> Perimeter field, which represents the floodplain—grid of the simulation, i.e., the perimeter where the hydraulic calculations will be carried out.
6. Grid generation, which contributes to the creation of the computational canvas and the selection of appropriate parameters to achieve optimal computational time. The selection of the dimensions of the canyon is based on the size of the area to be covered. In general, larger dimensions are preferred for larger areas in order to reduce the computational burden. The computational burden depends on the number of Computational Points to be created.
7. Input of structures is conducted in Ras Mapper from the SA/2D Connections layer. Incorporating structures into hydraulic simulations involves a systematic approach to accurately represent their impact on flow dynamics and flood behavior. This process starts with identifying and characterizing structures such as bridges, culverts, weirs, and dams based on their geometry, hydraulic properties, and operational conditions. These structures are then integrated into the hydraulic model, such as HEC-RAS, by placing them spatially within the model domain and specifying their attributes. The model calculates the structures' effects on flow characteristics, including velocity, water levels, and floodplain inundation extents. To adjust these structures, the upstream and downstream DEM's elevations are corrected according to the actual upstream and downstream elevation of each structure. Afterwards, all the geometric features of each structure, such as weir height and length, number of barrels, openings, etc., are assigned to the model. In this manner, the hydraulic model captures the discharge conveyed by each structure's hydraulic openings as well as the potential overflow.
8. Import Manning values as a shapefile.
9. The import of Boundary Conditions of their design is conducted through the Boundary Conditions layer. They are introduced either as a uniform flow along the stream flow for the streams covered by the sub-basin, or as an inflow upstream of the stream from an upstream sub-basin.
10. Import of hydrographs.

3. Results and Comparison

By simulating flow behavior under various scenarios, HEC-RAS enables the calculation of critical parameters such as water depths, flow velocities, and inundation areas. Results are presented per APSFR and per return period.

3.1. Hydrographs

HEC-RAS modeling generates detailed output hydrographs that are essential for understanding the temporal dynamics of flood events. These hydrographs depict how water flow parameters, such as discharge, water surface elevation, and velocity, change over time at specific locations within the study area.

3.1.1. APSFR 21–22

In the comparison of the results for each of the three return periods, T20, T100, and T500 years show a high identity of the flood peaks between full 2D and combined (1D/2D), which indicates the high convergence of the two methods.

According to Figure 3, a simulation of the 20-year flow hydrograph, a high identification of the flood peak between 2D and combined 1D/2D flood peaks can be observed. Specifically, 2D simulation predicts a flood peak of 142.74 m^3/s on September 1st at 14:00, identical to the peak predicted by the combined model at the same time, demonstrating the accuracy and reliability of the 2D simulation in replicating flood peak values.

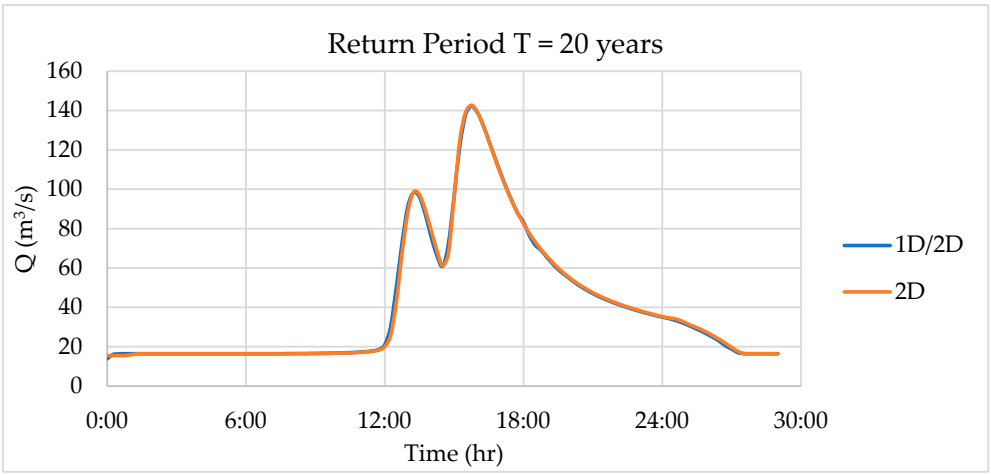

Figure 3. Comparison of hydrographs in the outlet of APSFR 21–22 for T = 20 years.

According to Figure 4, a simulation of the 100-year flow hydrograph, a high identification of the flood peak between 2D and combined 1D/2D flood peaks can be observed. Specifically, 2D simulation predicts a flood peak of 451.62 m^3/s on September 1st at 14:15, identical to the peak predicted by the combined model at the same time, demonstrating the accuracy and reliability of the 2D simulation in replicating flood peak values.

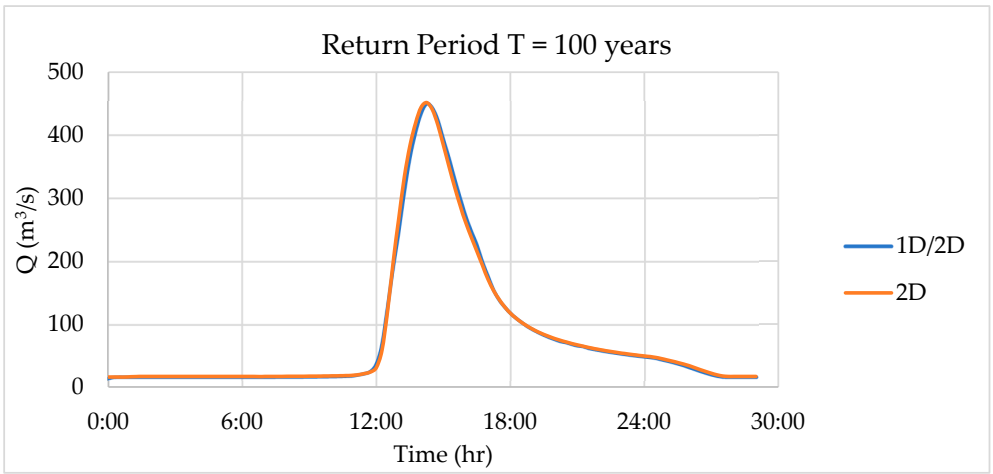

Figure 4. Comparison of hydrographs in the outlet of APSFR 21–22 for T = 100 years.

According to Figure 5, a simulation of the 500-year flow hydrograph, a high identification of the flood peak between 2D and combined 1D/2D flood peaks can be observed. Specifically, the 2D simulation predicts a flood peak of 687.53 m^3/s on September 1st at 15:45, identical to the peak predicted by the combined model at the same time, demonstrating the accuracy and reliability of the 2D simulation in replicating flood peak values.

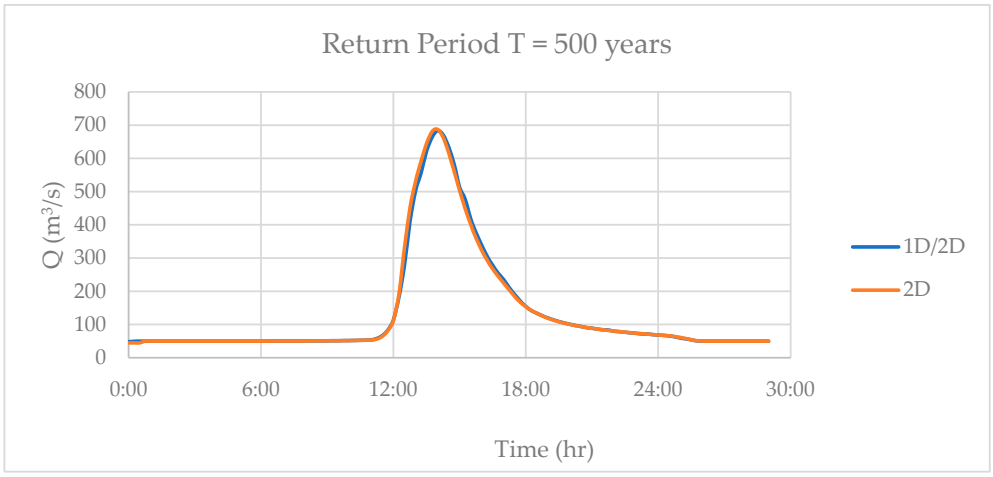

Figure 5. Comparison of hydrographs in the outlet of APSFR 21–22 for T = 500 years.

Figure 6 presents the initial 1D/2D model and the examined 2D model hydrographs, respectively. The selected location for APSFR 21–22 is one of the reported flooding incident areas in the confluence of the rivers (Location 1 is shown in the relevant Figure in Section 3.4.1). The following figure illustrates a high identification of the flood peak between 2D and combined 1D/2D flood peaks. Specifically, 1D/2D simulation predicts a slightly higher flood peak, which comes in agreement with the difference in the inundated area shown in Table 2.

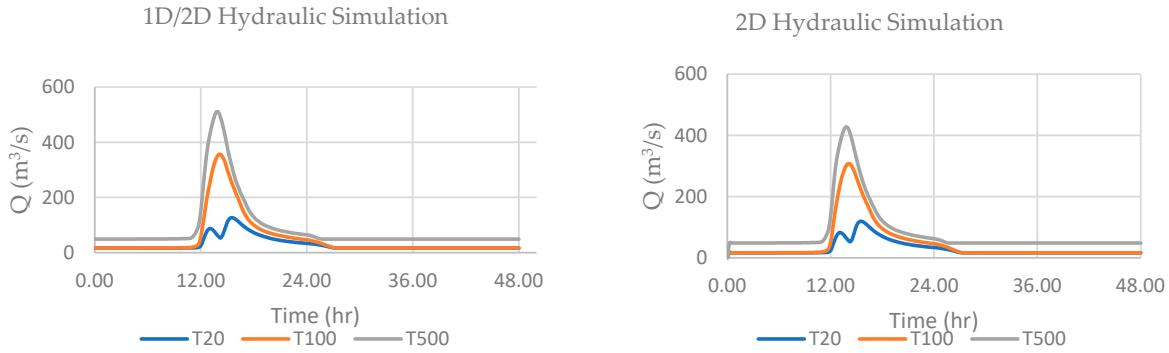

(**a**) (**b**)

Figure 6. (**a**) Hydrographs in Location 1 for APSFR 21–22, (**b**) hydrographs in Location 1 for APSFR 29.

Table 2. Percentage difference in inundated area.

Hydraulic Model	Return Period (Years)	Inundated Area (km^2) 1D/2D	Inundated Area (km^2) 2D	Difference in Percentage
APSFR 21–22	T20	0.17	0.20	13%
	T100	0.29	0.29	2%
	T500	0.31	0.31	−1%
APSFR 29	T20	0.72	0.82	12%
	T100	0.97	1.03	6%
	T500	1.11	1.18	6%

3.1.2. APSFR 29

According to Figure 7, in the hydraulic simulation of a 20-year return period event, a notable agreement between the flood peaks of the full 2D and combined 1D/2D model was observed. The 2D simulation produced a flood peak of 56.12 m^3/s at 14 h and 45′ from the start of the event, while the combined model indicated a flood peak of 65.31 m^3/s at 14 h and 40′. The difference of 14% in flood peaks is deemed reasonable and aligns with the results presented in Table 2, which recorded the largest runoff volume error at 5.2%. This discrepancy can be attributed to the retention of water approximately 580 m upstream of the outlet, which prevents this volume from reaching the outlet. This retention is likely due to the agricultural land in the area, which affects the flow dynamics. Additionally, the accuracy of the calculation and the detailed design of the computational grid, which can be adjusted by the user, contribute to this result.

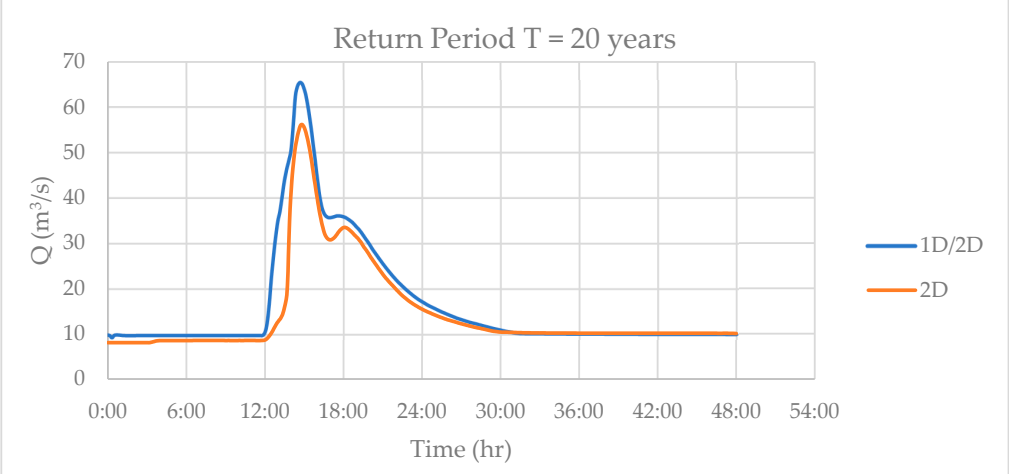

Figure 7. Comparison of hydrographs in the outlet of APSFR 29 for T=20 years.

According to Figure 8, in the hydraulic simulation of the 100-year return period, a high match of the flood peak between full 2D and combined 1D/2D flood peaks is observed. The 2D simulation gives a flood peak at 14 h 30′ from the event occurrence and is equal to 110.02 m^3/s. The combined one at 14 h 20′ is equal to 115.44 m^3/s. Therefore, there is a high convergence between the peak flows and the occurrence of small discrepancies considered non-critical.

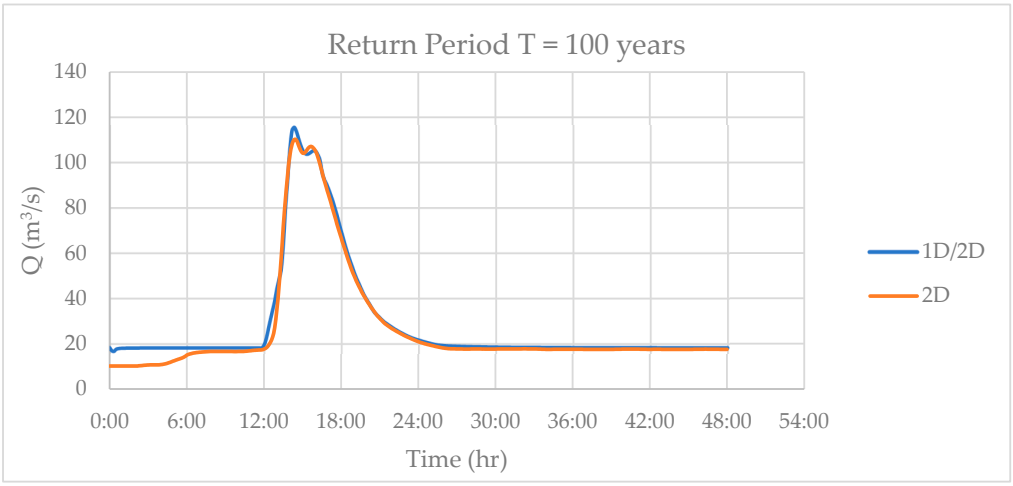

Figure 8. Comparison of hydrographs in the outlet of APSFR 29 for T = 100 years.

According to Figure 9, in the hydraulic simulation of the 500-year return period, a high correlation between the flood peaks of the full 2D and combined 1D/2D models was observed. The 2D simulation indicated a flood peak of 198.2 m^3/s at 15 h and 15 min from the start of the event, while the combined model predicted a flood peak of 196.83 m^3/s at 15 h. The close alignment of peak flows, with a negligible time lag, underscores the reliability and accuracy of both modeling approaches.

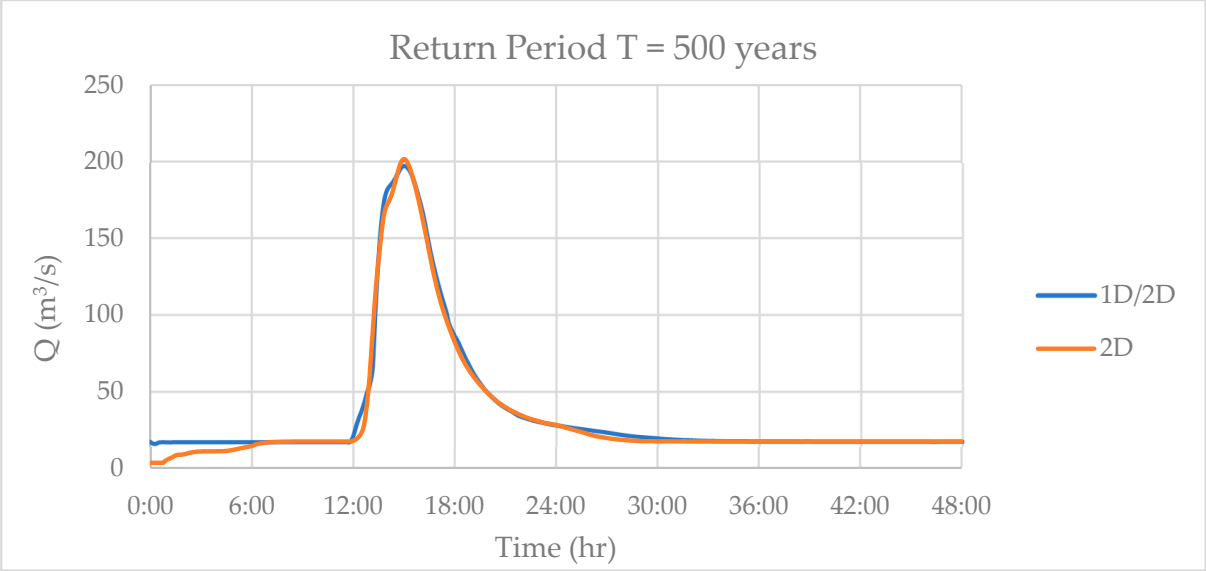

Figure 9. Comparison of hydrographs in the outlet of APSFR 29 for T = 500 years.

Figure 10 presents the initial 1D/2D model and the examined 2D model hydrographs. The selected location for APSFR 29 is one of the reported flooding incident areas near the University of Cyprus campus affecting many facilities (Figure 20 is shown in Location 1). The following figure shows a high identification of the flood peak and the time from the event occurrence and between the 2D and combined 1D/2D flood peaks.

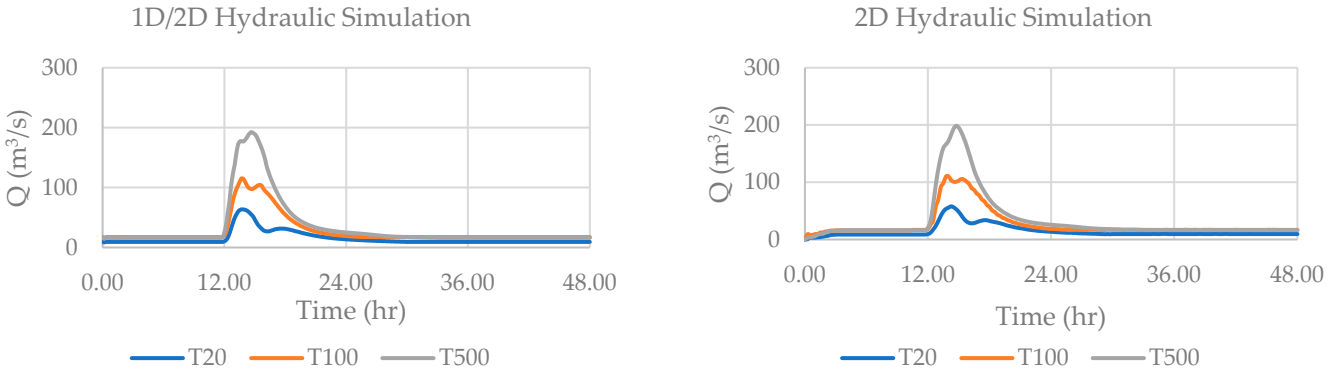

(**a**) (**b**)

Figure 10. (**a**) Hydrograph in Location 1 for APSFR 29, (**b**) hydrograph in Location 1 for APSFR 29.

Regarding the results, there is an agreement between the flood peak values and their occurrence in the full two-dimensional and the combined 1D/2D hydraulic simulations. A higher convergence of hydrographs was observed in the hydraulic simulation of the APSFR 21–22, constituting an area of higher slopes compared to APSFR 29.

3.2. Inundation Maps

By simulating water surface profiles and flow patterns, HEC-RAS generates detailed maps that depict the extent and depth of flooding under various scenarios, such as different storm intensities or infrastructure failures. A flood field is considered to be a piece of land within the channel that is covered by water. These maps are instrumental for urban planning, emergency response, and floodplain management, as they provide clear, spatially resolved information on potential inundation areas, contributing to the identification of vulnerable regions, planning evacuation routes, and designing flood mitigation structures.

Thus, a criterion of comparison for this thesis is the flooding areas of the two different hydraulic methods (2D and combined 1D/2D). The extraction of the fields is carried out in HEC-RAS through the results for each return period T = 20, 100, and 500 years in each APSFR. Table 2 illustrates inundated areas for each hydraulic model, scenario, and methodology.

3.2.1. APSFR 21–22

Comparing the inundation area maps produced by the 1D/2D combined hydraulic simulation method and the full 2D method, no notable differences were noticed. The following inundated maps (Figures 11–13) present the flooding area in APSFR 21–22 for each return period, T = 20, 100, and 500 years, respectively. These results came into agreement with the hydrographs that are explained in Section 3.1. In smaller flooding areas, greater percentage differences are observed.

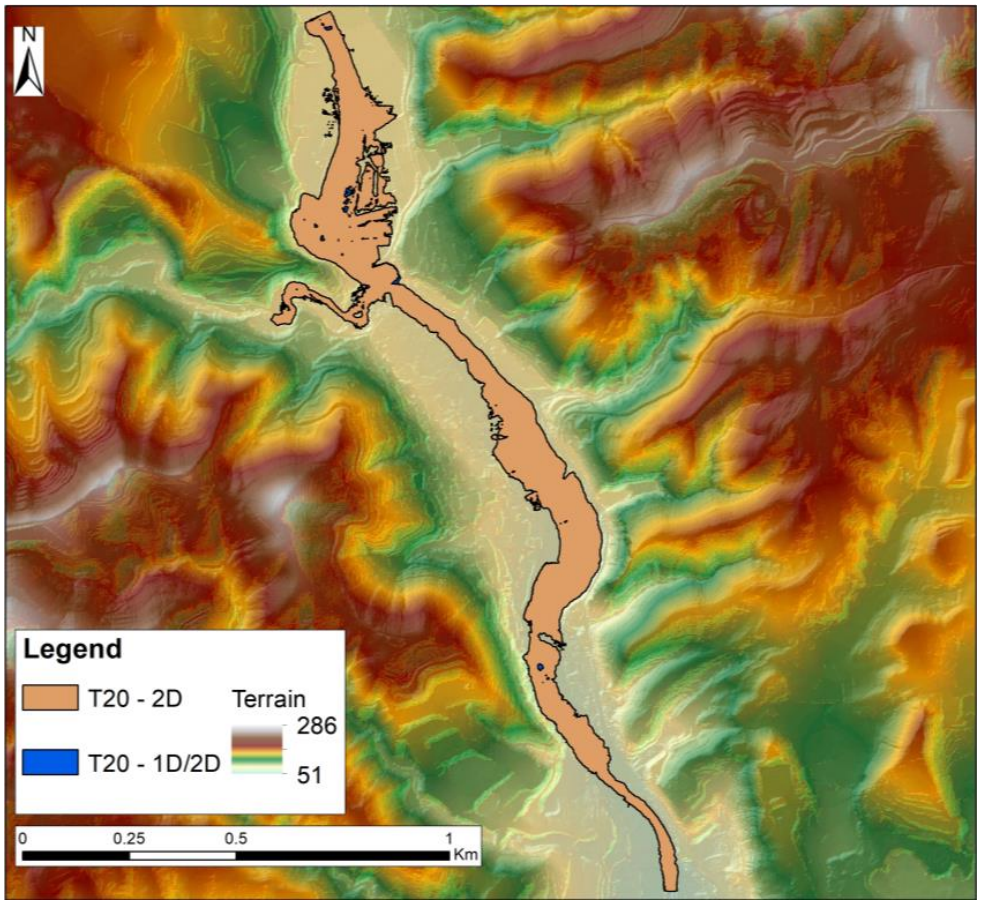

Figure 11. Comparison of inundation maps in APSFR 21–22 for T = 20 years.

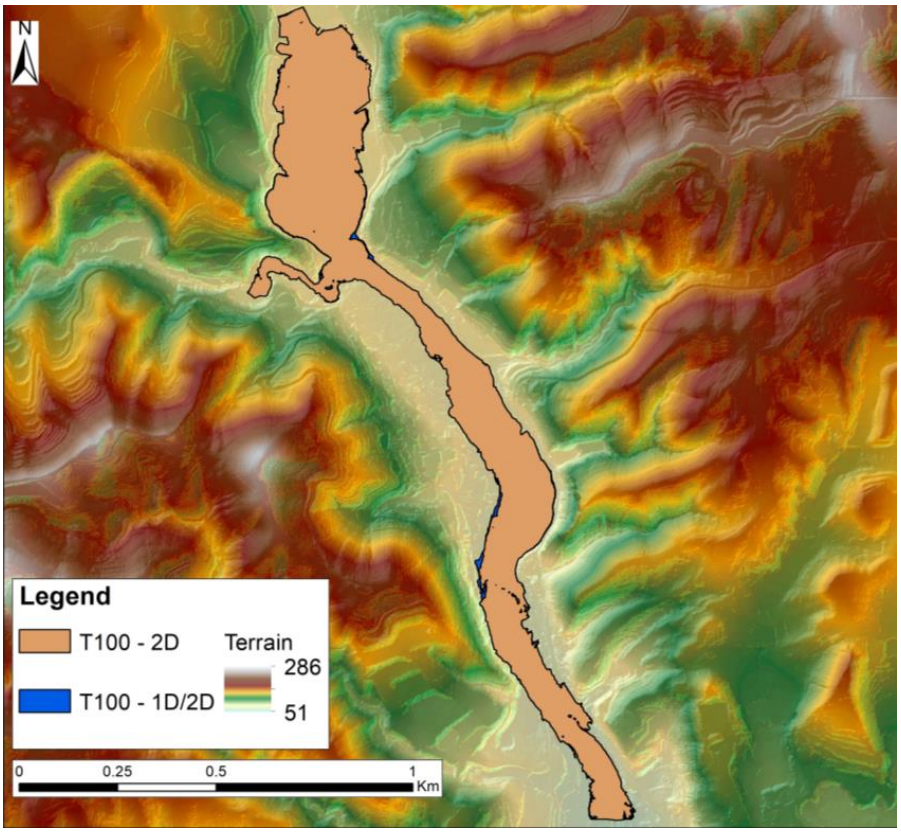

Figure 12. Comparison of inundation maps in APSFR 21–22 for T = 100 years.

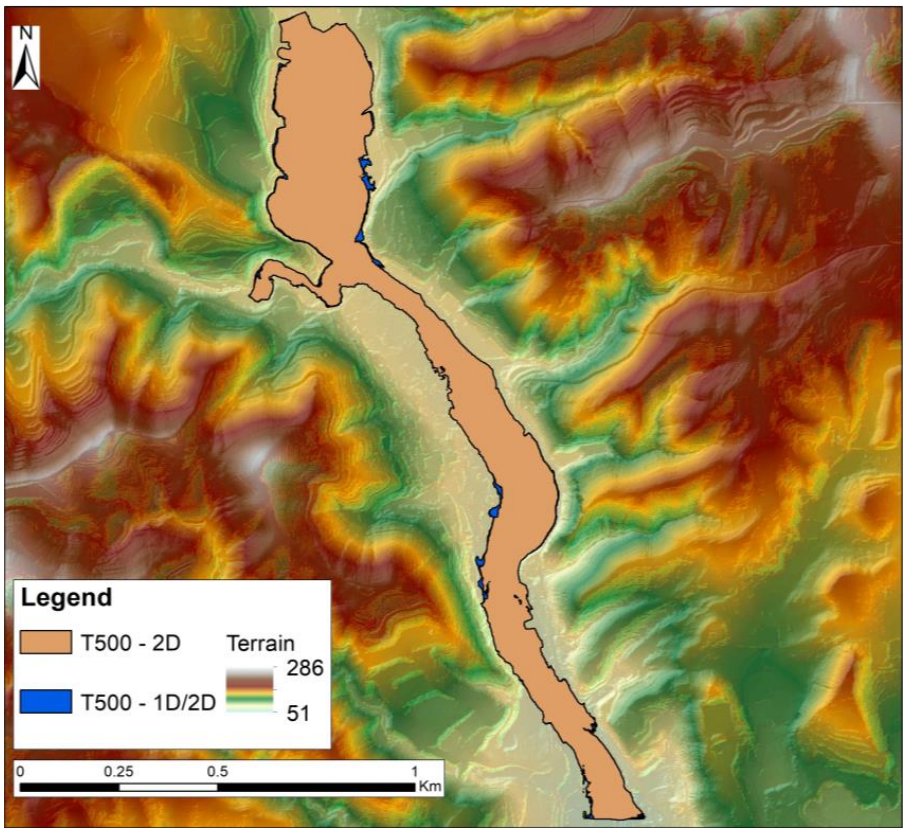

Figure 13. Comparison of inundation maps in APSFR 21–22 for T = 500 years.

For comparative purposes, floodplain maps were generated for each method, 1D/2D and 2D, for each return period. These maps provide a visual representation of the estimated floods and allow for the analysis and evaluation of the differences between the modeling methods. This comparison is crucial for understanding the impact of each method on the accuracy and reliability of flood predictions. The following Figure 14 presents inundation boundaries that are quite similar for both simulation methods, 1D/2D and 2D. Any minor areas of inundation are attributed to the presence of agricultural lands where water tends to accumulate rather than flow downstream. This similarity indicates that both methods produce comparable results in predicting flood extents, with variations primarily influenced by local land use and topography.

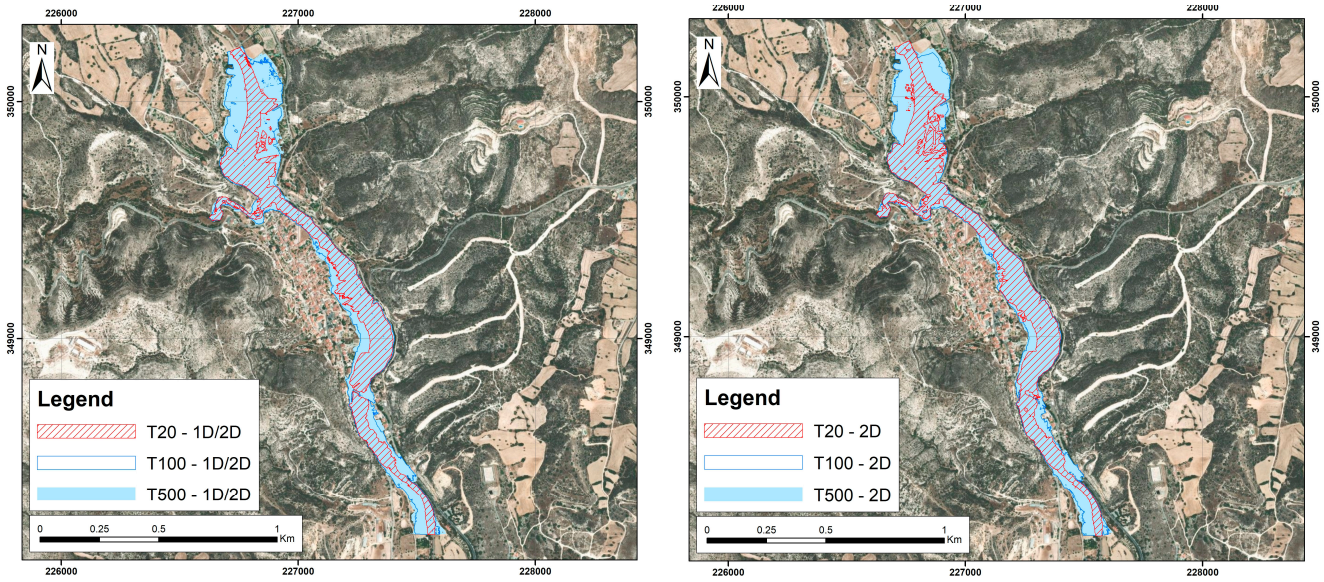

(**a**) (**b**)

Figure 14. (**a**) Inundated area in APSFR 21–22 for combined 1D/2D simulation, (**b**) inundated area in APSFR 21–22 for full 2D simulation.

3.2.2. APSFR 29

Inundation maps showing the spatial distribution of accuracy and omission and commission errors are shown in Figures 15–17. In comparison to maps of APSFR 21–22, these maps show a slight deviation between the flood extents observed, as presented below. Such minor discrepancies are considered reasonable and are attributed to the computational accuracy selected for the specific models. Additionally, these discrepancies may be due to varying land uses (higher Manning's coefficient), especially in agricultural areas that show areal water retention.

The full 2D model generally provides a more detailed representation of flood extents, capturing complex flow patterns and interactions with terrain features more accurately than the 1D/2D method. This results in a higher-resolution map with finer details in areas of variable topography. In contrast, the 1D/2D model, while computationally less intensive, may smooth out some of these details, leading to a less precise delineation of flood boundaries, especially in areas with abrupt changes in elevation or complex flow paths.

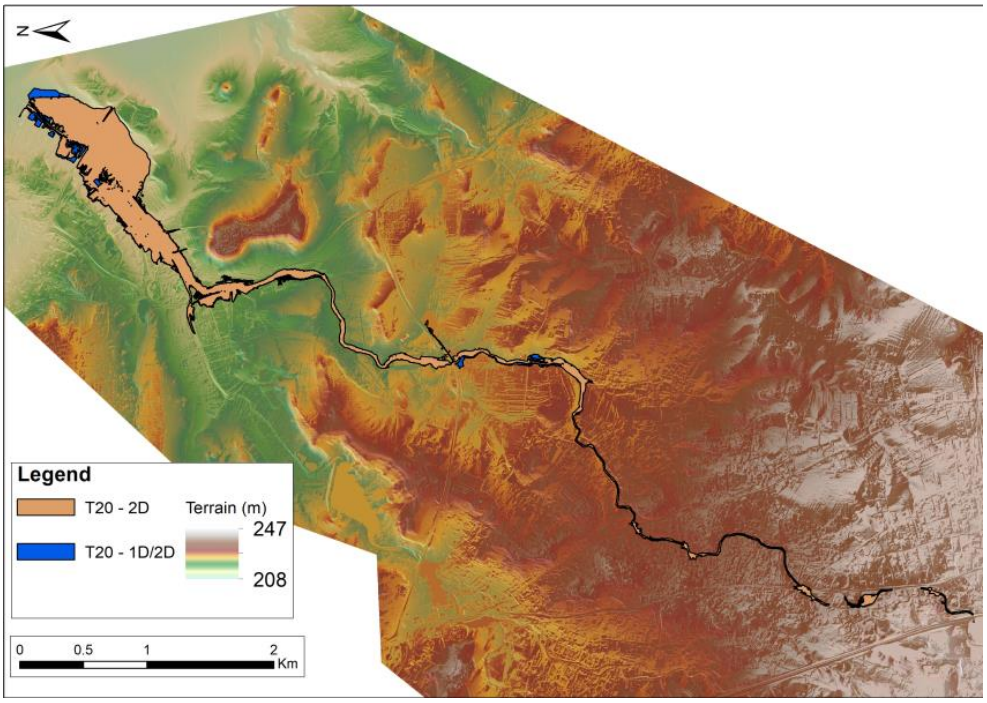

Figure 15. Comparison of inundation maps in APSFR 29 for T = 20 years.

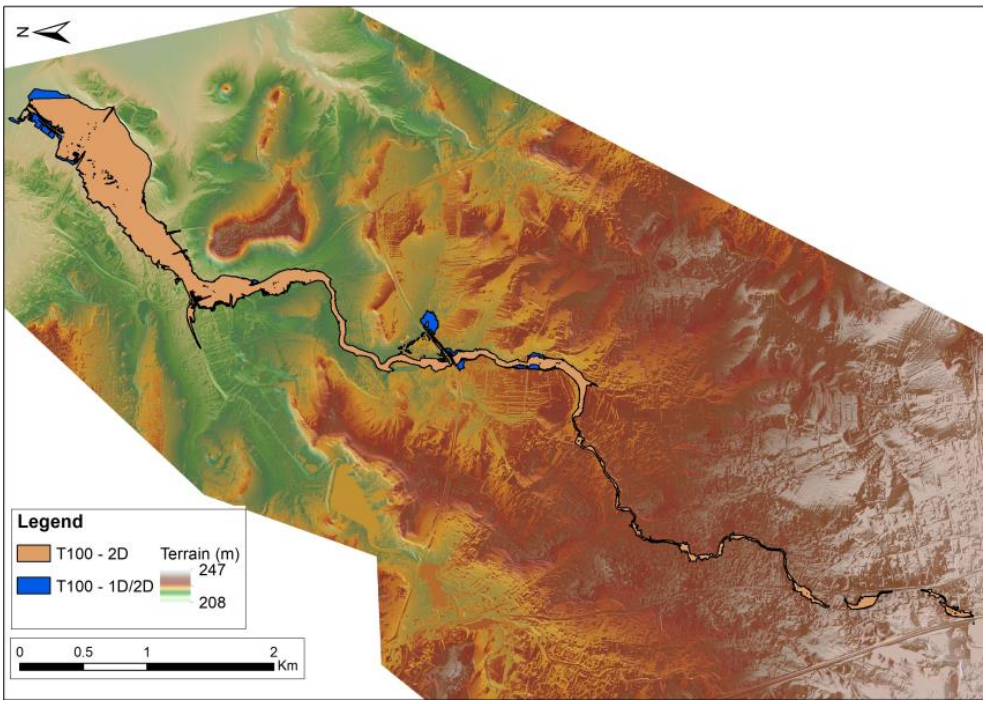

Figure 16. Comparison of inundation maps in APSFR 29 for T = 100 years.

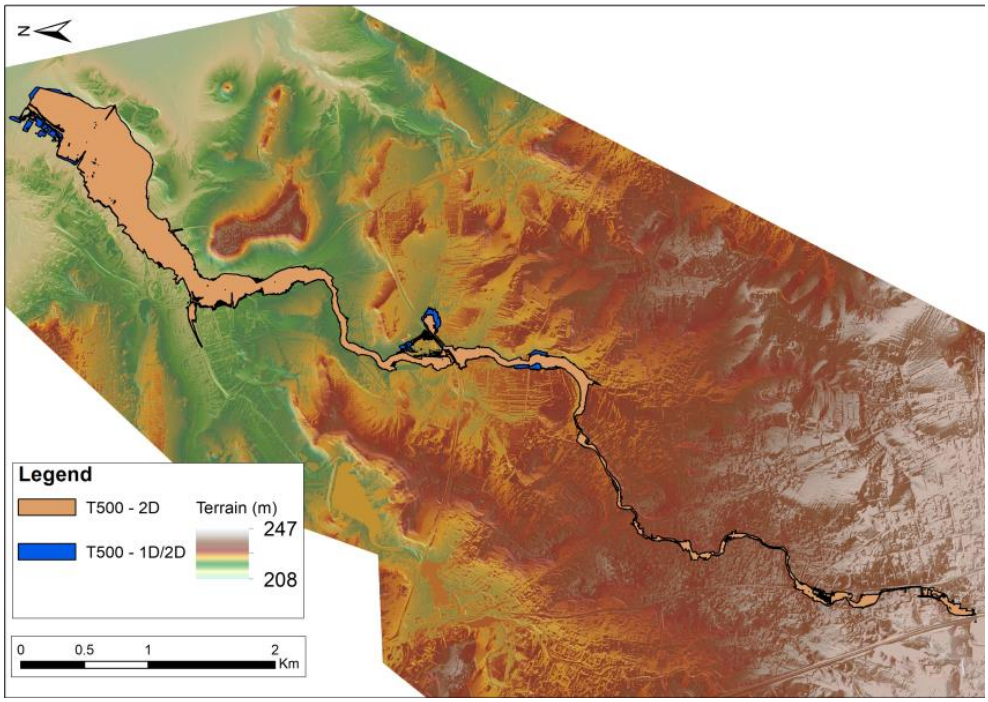

Figure 17. Comparison of inundation maps in APSFR 29 for T = 500 years.

For comparative purposes, floodplain maps were generated for each method, 1D/2D and 2D, for each return period. These maps provide a visual representation of the estimated floods and allow for the analysis and evaluation of the differences between the modeling methods. This comparison is crucial for understanding the impact of each method on the accuracy and reliability of flood predictions. Figure 18 presents inundation boundaries that are quite similar for both simulation methods, 1D/2D and 2D. Any minor areas of inundation are attributed to the presence of agricultural lands, where water tends to accumulate rather than flow downstream. This similarity indicates that both methods produce comparable results in predicting flood extents, with variations primarily influenced by local land use and topography.

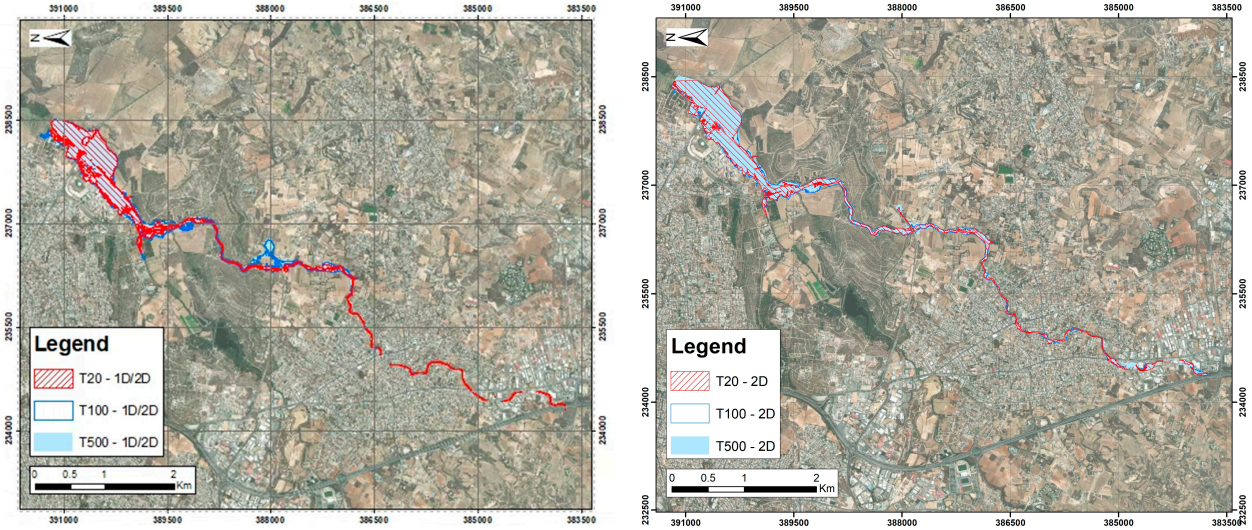

(**a**) (**b**)

Figure 18. (**a**) Inundated area in APSFR 29 for combined 1D/2D simulation, (**b**) inundated area in APSFR 29 for full 2D simulation.

3.3. Simulation Time

Another parameter taken into account was the simulation and development time of both hydraulic models. As supporting studies show [22], 1D/2D models are time consuming for the building of the model, taking about 7–10 days for each model. As for the hydraulic simulation time, by comparison, it only takes 2 days for the 2D models. As the following Tables 3 and 4 show, the 2D simulation time might take longer than 1D/2D, although in terms of total time, the 2D method is better.

Table 3. Comparison between simulation time and volume error in APSFR of 2D hydraulic simulation.

Hydraulic Model	Return Period (Years)	Volume Error (%)	Simulation Time (h)
APSFR 21–22	T20	−0.11	04:22:25
	T100	0.05	04:05:09
	T500	0.00	01:51:39
APSFR 29	T20	3.20	17:35:58
	T100	2.95	13:54:16
	T500	1.62	09:20:53

Table 4. Comparison between simulation time and volume error in APSFR of 1D/2D hydraulic simulation.

Hydraulic Model	Return Period (Years)	Simulation Time (h)
APSFR 21–22	T20	02:05:12
	T100	02:12:36
	T500	02:37:04
APSFR 29	T20	02:18:28
	T100	02:41:22
	T500	02:51:07

3.4. Depth Maps

The extraction of depth results through HEC-RAS was a fundamental part of this study. HEC-RAS 6.3.1 software offers robust capabilities for displaying and analyzing water depths, which is essential for flood risk management and hydraulic modeling. Tables 5 and 6 show statistics of depth outputs that are in agreement with the inundation maps and the flooding area differences between the two methods. In general, these differences between the methods are acceptable and not critical. Max values of depth (>6 m) are explained by a wide area of agricultural uses.

Table 5. Statistics of depths in 2D hydraulic simulation.

	APSFR 21–22			APSFR 29		
	T20	**T100**	**T500**	**T20**	**T100**	**T500**
Max	4.29	6.22	6.81	6.28	6.55	6.68
Mean	1.07	1.62	0.00	0.58	0.69	0.80
Min	0.00	0.00	2.21	0.00	0.00	0.00
Stdev	0.83	1.14	1.38	0.57	0.62	0.66

Using the hydraulic simulation capabilities of HEC-RAS, detailed maps were generated depicting the spatial distribution of water depths across the study area. These maps include specific locations, designated as Positions 1, 2, and 3, where flood events have been reported, as analyzed in Section 2.1. Highlighting these areas with historical flood occurrences provides valuable insights into the flood behavior of the region and supports the development of effective flood risk management strategies.

Table 6. Statistics of depths in combined 1D/2D hydraulic simulation.

	APSFR 21–22			APSFR 29		
	T20	**T100**	**T500**	**T20**	**T100**	**T500**
Max	3.65	5.69	6.81	6.39	6.00	6.00
Mean	0.98	1.70	2.21	0.64	0.75	0.84
Min	0.00	0.00	0.00	0.00	0.00	0.00
Stdev	0.76	1.20	1.38	0.61	0.67	0.73

3.4.1. Depth Maps of APSFR 21–22

The following Figure 19 illustrates the max depths of APSFR 21–22 for each return period of 20, 100, and 500 years, respectively. Comprehensive maps that depict the maximum flood depths obtained from each method facilitate a direct visual comparison. Also, locations reported for flooding incidents are shown. A high degree of congruence between the two simulation methods is revealed, suggesting that both approaches are capable of producing reliable predictions of flood extents and depths. These findings underscore the robustness of the combined 1D/2D approach while highlighting the enhanced spatial resolution and detail achievable with fully 2D simulation.

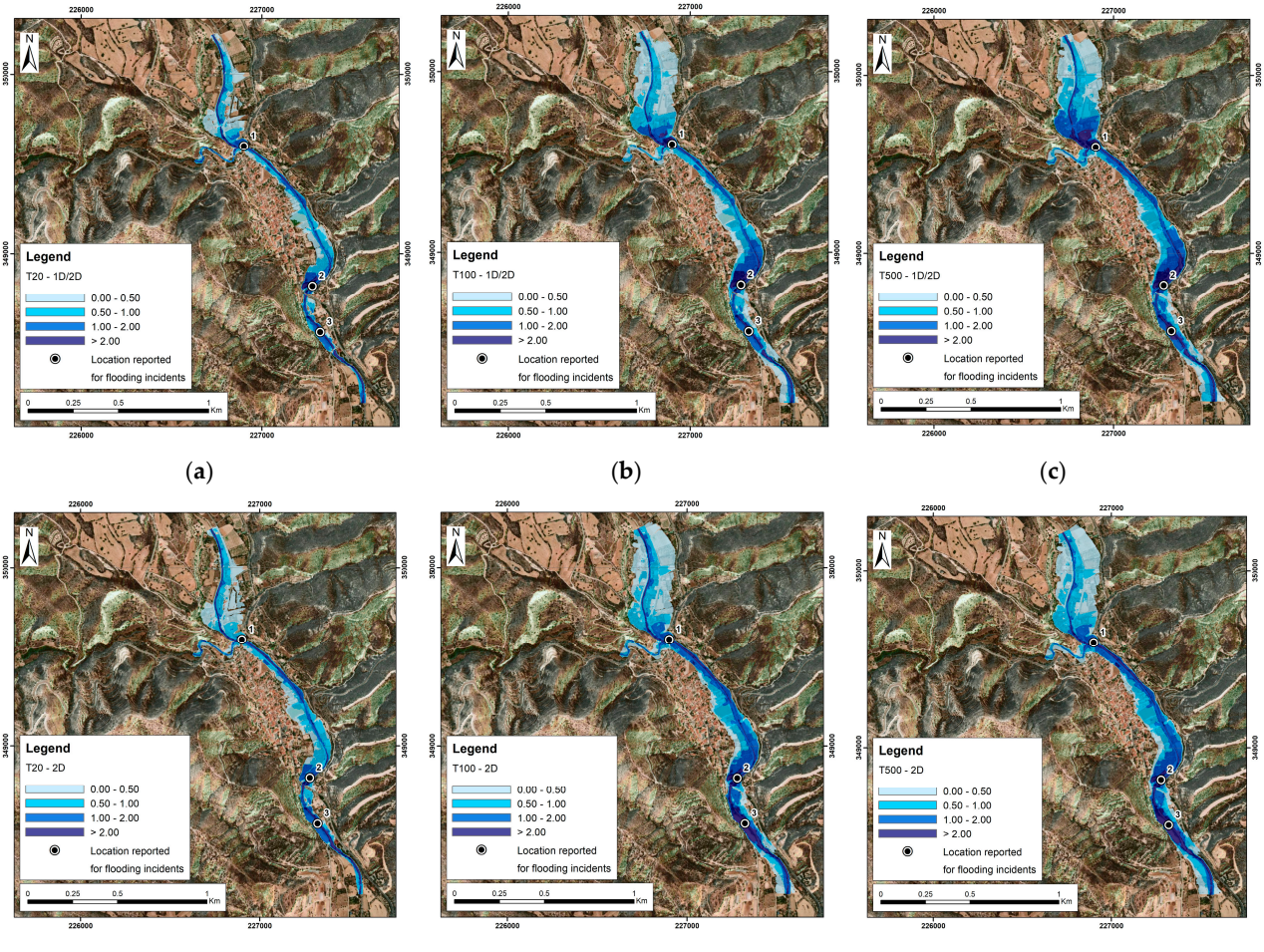

Figure 19. (**a**) Depth map for T = 20 years for 1D/2D hydraulic simulation, (**b**) depth map for T = 100 years for 1D/2D hydraulic simulation, (**c**) depth map for T = 500 years for 1D/2D hydraulic simulation, (**d**) depth map for T = 20 years for 2D hydraulic simulation, (**e**) depth map for T = 100 years for 2D hydraulic simulation, (**f**) depth map for T = 500 years for 2D hydraulic simulation.

3.4.2. Depth Maps of APSFR 29

Figure 20 illustrates the max depths of APSFR 29 for each return period of 20, 100, and 500 years, respectively. Comprehensive maps that depict the maximum flood depths obtained from each method facilitate a direct visual comparison. Also, locations reported for flooding incidents are shown. A high degree of congruence between the two simulation methods is revealed, suggesting that both approaches are capable of producing reliable predictions of flood extents and depths. These findings underscore the robustness of the combined 1D/2D approach while highlighting the enhanced spatial resolution and detail achievable with fully 2D simulation.

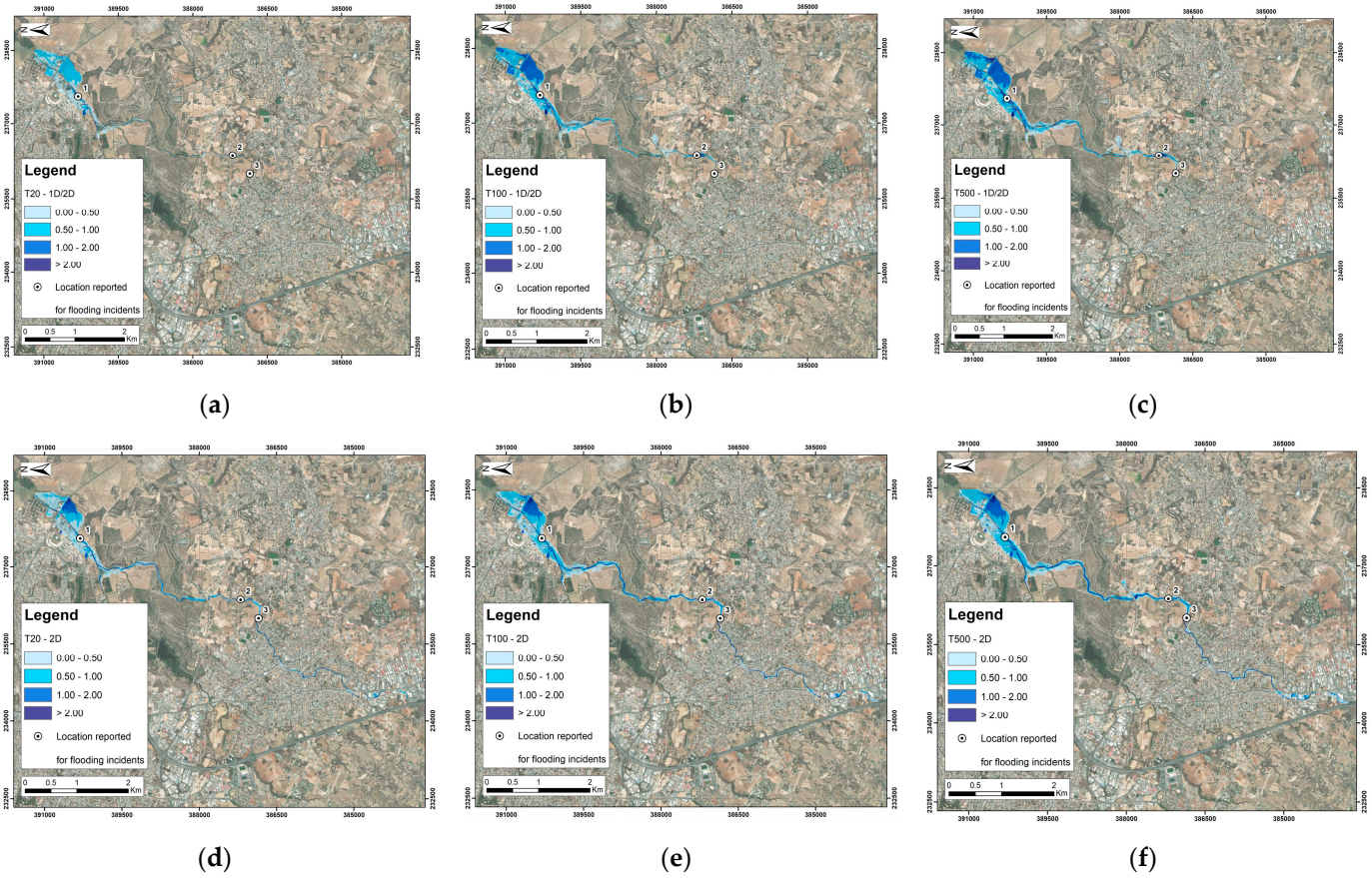

Figure 20. (**a**) Depth map for T = 20 years for 1D/2D hydraulic simulation, (**b**) depth map for T = 100 years for 1D/2D hydraulic simulation, (**c**) depth map for T = 500 years for 1D/2D hydraulic simulation, (**d**) depth map for T = 20 years for 2D hydraulic simulation, (**e**) depth map for T = 100 years for 2D hydraulic simulation, (**f**) depth map for T = 500 years for 2D hydraulic simulation.

3.5. Velocity Maps

The extraction of velocity results through HEC-RAS was a crucial component of this study. Using the hydraulic simulation capabilities of HEC-RAS, detailed maps were generated depicting the spatial distribution of flow velocities across the study area. The identification of these high-velocity zones is essential for understanding the hydrodynamic behavior of the river system and for implementing effective flood risk management strategies. The following figures highlight specific locations for APSFR 21–22 and 29, respectively. Elevated velocity values were observed, particularly within the river channel.

3.5.1. Velocity Maps of APSFR 21–22

Figure 21 illustrates velocities across the study area for each hydraulic simulation method (combined 1D/2D and full 2D) and each return period, with comprehensive

maps that depict the velocity distributions obtained from each method, facilitating a direct visual comparison of areas with elevated velocities as well as the entire region of interest. Figures (a–c) and (d–f) show return periods of 20, 100, and 500 years, respectively. Indicatively, areas with higher velocities in the riverbed are emphasized. Analysis revealed a high degree of congruence between the two simulation methods, both in the overall velocity distribution and in identifying specific locations of high velocities. These findings underscore the robustness of the 1D/2D hybrid approach while highlighting the enhanced spatial resolution and detail achievable with fully 2D simulations.

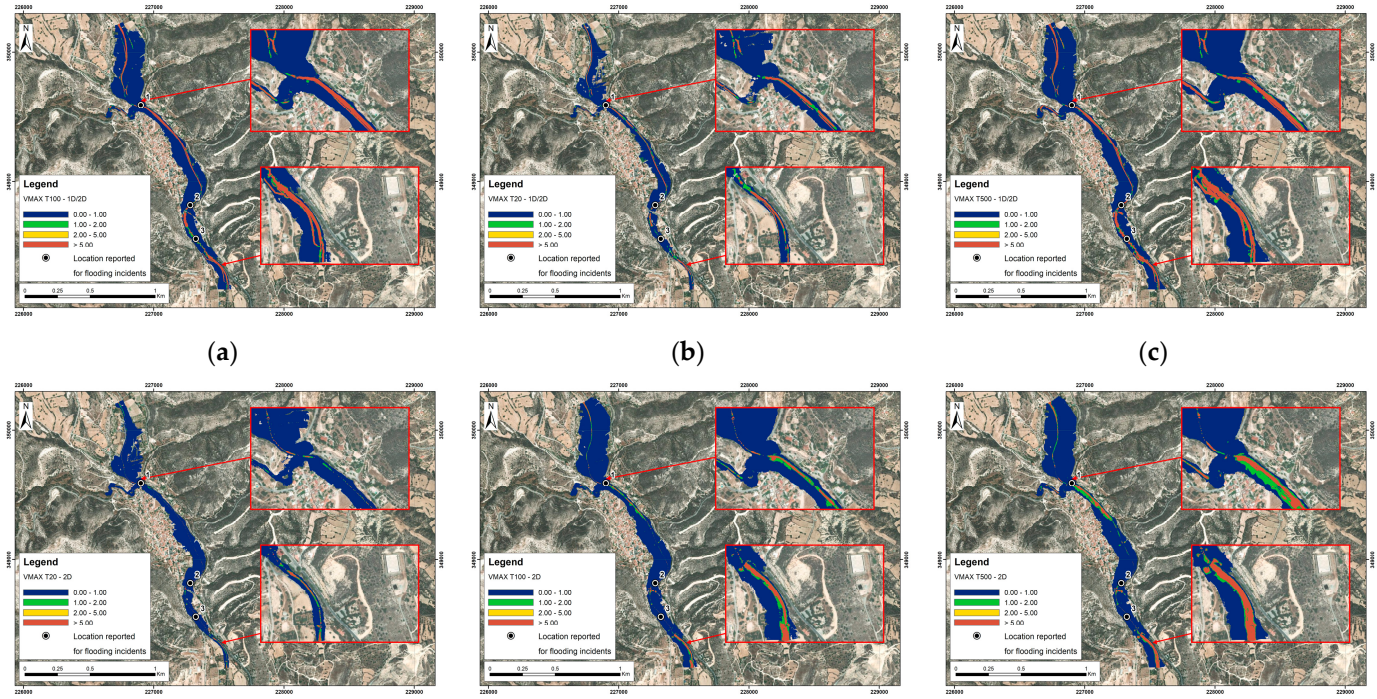

Figure 21. (**a**) Velocity map for T = 20 years for 1D/2D hydraulic simulation, (**b**) velocity map for T = 100 years for 1D/2D hydraulic simulation, (**c**) velocity map for T = 500 years for 1D/2D hydraulic simulation, (**d**) velocity map for T = 20 years for 2D hydraulic simulation, (**e**) velocity map for T = 100 years for 2D hydraulic simulation, (**f**) velocity map for T = 500 years for 2D hydraulic simulation.

3.5.2. Velocity Maps of APSFR 29

Figure 22 illustrates velocities across the study area for each hydraulic simulation method (combined 1D/2D and full 2D) and each return period, with comprehensive maps that depict the velocity distributions obtained from each method, facilitating a direct visual comparison of areas with elevated velocities as well as the entire region of interest. Figures (a–c) and (d–f) show return periods of 20, 100, and 500 years, respectively. Indicatively, areas with higher velocities in the riverbed are emphasized. Analysis revealed a high degree of congruence between the two simulation methods, both in the overall velocity distribution and in identifying specific locations of high velocities. These findings underscore the robustness of the 1D/2D hybrid approach while highlighting the enhanced spatial resolution and detail achievable with fully 2D simulations.

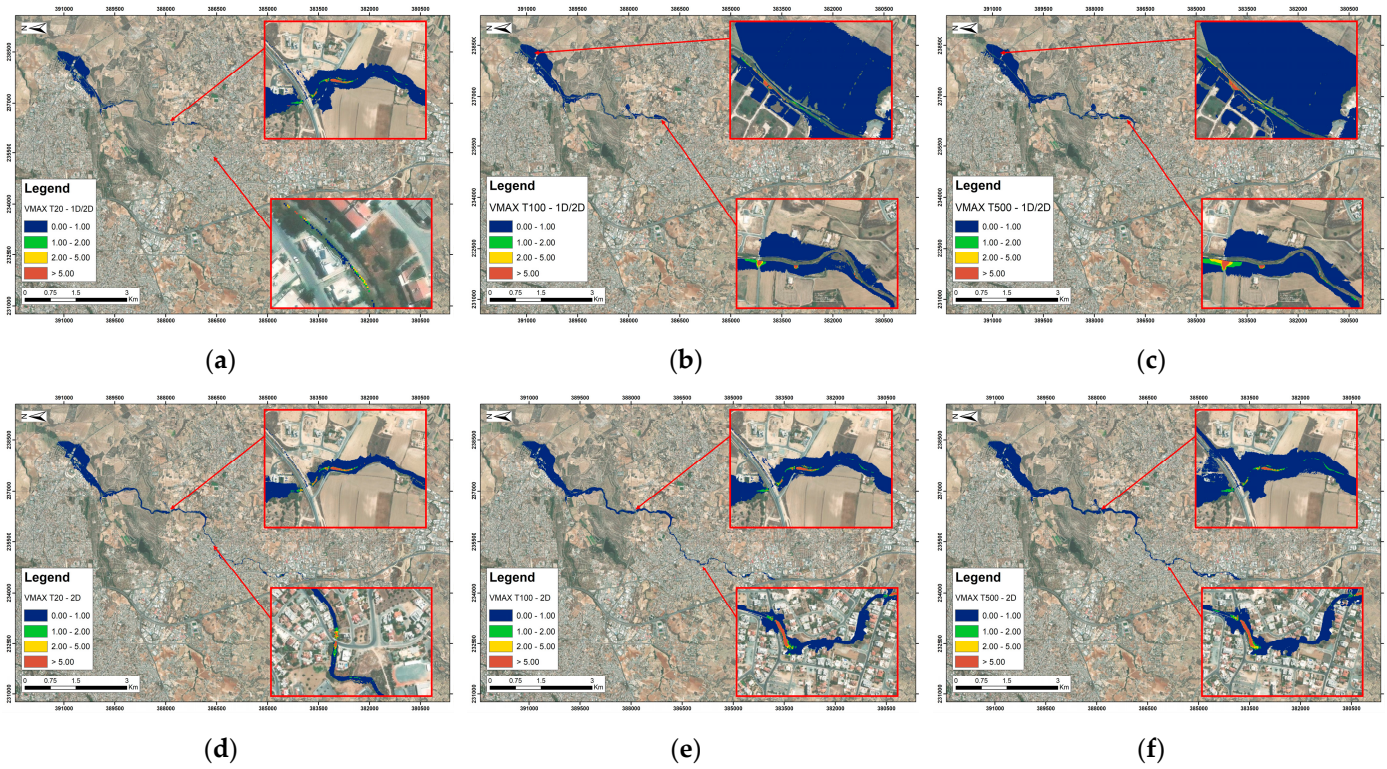

Figure 22. (**a**) Velocity map for T = 20 years for 1D/2D hydraulic simulation, (**b**) velocity map for T = 100 years for 1D/2D hydraulic simulation, (**c**) velocity map for T = 500 years for 1D/2D hydraulic simulation, (**d**) velocity map for T = 20 years for 2D hydraulic simulation, (**e**) velocity map for T = 100 years for 2D hydraulic simulation, (**f**) velocity map for T = 500 years for 2D hydraulic simulation.

4. Discussion and Conclusions

Floods can pose risks to both human life and the environment, necessitating robust measures for effective management and mitigation. The European Union's Directive 2007/60/EC on the assessment and management of flood risks provides a framework to reduce and manage these risks through comprehensive planning and preventive actions [1]. In Cyprus, rainfall patterns can lead to severe flooding events, particularly in urban areas with inadequate drainage systems. The implementation of Directive 2007/60/EC in Cyprus involves identifying areas at significant risk and developing Flood Risk Management Plans (FRMPs) tailored to these zones. Hydraulic simulation plays a crucial role in this process by providing detailed models of flood behavior, helping to predict flood extents, depths, and velocities. These simulations support the development of effective FRMPs, ensuring that appropriate measures are taken to minimize the impact of flooding on vulnerable areas. The accuracy of flood prediction is crucial for the proper mitigation of flooding effects on people, infrastructure, and the environment.

Hydraulic simulation plays a key role in this purpose. The present research successfully investigated the two different behaviors between combined 1D/2D and full 2D models applying HEC-RAS 2D in two existing designated areas of potential flooding in Cyprus.

Specifically, the behavior and the results of the two different hydraulic modeling approaches were compared. The main findings of this research are summarized below:

- Two-dimensional simulation provides a more accurate representation of complex and high flow conditions and hydraulic behavior.
- Hydraulic models based on a fully two-dimensional grid show higher capabilities of capturing inundation areas where high slopes are present or in cases of flooding in numerous directions.
- The 2D hydraulic simulation offers greater flexibility in modeling various hydraulic scenarios, such as urban and riverine flooding and hydraulic structure adaptions,

making it suitable for a wide range of applications, alternative solutions, and enhanced resilience planning.

- The 2D model is found to be more stable compared to the 1D/2D approach, where significant instabilities and computational errors are common.

Hydraulic modeling using the 1D/2D approach remains highly effective in various scenarios, as stated by recent research [35–37]. The combined 1D/2D approach excels in environments with complex geometries, such as urban areas and intricate river systems, where it combines the strengths of both 1D and 2D modeling techniques. Recent studies highlight its efficiency in large-scale watershed simulations, where the 1D component efficiently handles extensive river networks, while the 2D component accurately captures floodplain dynamics [38]. In urban flood scenarios, the 1D/2D method effectively models both the drainage network and surface flooding, providing a detailed and accurate representation of urban hydrodynamics. This method is also advantageous in scenarios requiring rapid simulations, such as real-time flood forecasting, due to its balance between computational efficiency and spatial accuracy [39]. Moreover, the 1D/2D approach facilitates the evaluation of flood mitigation measures by allowing efficient scenario analysis and detailed spatial representation [40]. Consequently, the 1D/2D modeling method is considered suitable for complex river systems, large watersheds, urban flood scenarios, and comprehensive flood risk assessments.

However, the rapid development of home or office computer capabilities has pushed current practice toward the full 2D approach [41,42], whereas already noted by the present research, many advantages are attributed when compared to the interim 1D/2D approach. Contemporary research has already noted the efficiency of 2D HEC-RAS in modeling urban flooding and suggested its incorporation in early warning systems or other flood management practices [43]. Additionally, 2D modeling flood extents have been compared to satellite imagery of severe flooding and validated accordingly [41]. Similar research has additionally validated the performance of 2D HEC-RAS modeling regarding flood depths, discharge, and velocities against delicate and secluded modeling software [44].

Returning to the findings of the present research, full 2D modeling showed high identification results, with the approval of the Cypriot authorities, for combined 1D/2D hydraulic simulations, as far as inundation, discharge, flood depths, and velocities are concerned [45]. In conclusion, the 2D approach is found to be capable of successfully capturing the flooding incident of different return periods, from common to rare events. Moreover, its greater ease of use and the fact it is less prone to computational errors nature compared to the 1D/2D approach, contribute to the suggestion for broader usage of the 2D HEC-RAS methodology presented for flood management. Additionally, the authors highlight the importance of validation with ground measurements, which was not possible in the present case. It is suggested for future research to follow the presented methodology for 2D modeling in a country and a river system with sufficient in situ data in order to provide further evidence for the efficiency of 2D hydraulic modeling.

Author Contributions: Conceptualization, G.S. and N.G.; methodology, G.S.; software, G.S. and N.G.; validation, N.G. and E.B.; formal analysis, G.S. and N.G.; investigation, G.S.; resources, G.S. and E.B.; data curation, G.S.; writing—original draft preparation, G.S.; writing—review and editing, N.G. and E.B.; visualization, G.S.; supervision, E.B. All authors have read and agreed to the published version of the manuscript.

Funding: This research received no external funding.

Data Availability Statement: Specific data are available upon request from Water Development Department, as specified in Section 2.2.

Acknowledgments: We would like to express our gratitude to the Water Development Department of Cyprus for providing us with the data of the second FRMP cycle.

Conflicts of Interest: The authors declare no conflicts of interest.

References

1. EUR-Lex Directive—2007/60—EN—EUR-Lex. Available online: https://eur-lex.europa.eu/legal-content/EN/ALL/?uri=celex:32007L0060 (accessed on 24 May 2024).
2. Farsangi, E.N. *Natural Hazards: Impacts, Adjustments and Resilience*; Books on Demand: Norderstedt, Germany, 2021.
3. UNDRR. *An Overview of the Last 20 Years*; UNDRR: Geneva, Switzerland, 2019.
4. Uncounted Costs—Data Gaps Hide the True Human Impacts of Disasters in 2023 | UNDRR. Available online: https://www.undrr.org/explainer/uncounted-costs-of-disasters-2023 (accessed on 11 May 2024).
5. Chenoweth, J.; Hadjinicolaou, P.; Bruggeman, A.; Lelieveld, J.; Levin, Z.; Lange, M.A.; Xoplaki, E.; Hadjikakou, M.; Chenoweth, C.; Hadjinicolaou, P.; et al. Impact of Climate Change on the Water Resources of the Eastern Mediterranean and Middle East Region: Modeled 21st Century Changes and Implications. *Water Resour. Res.* **2011**, *47*, 6506. [CrossRef]
6. Tramblay, Y.; Arnaud, P.; Artigue, G.; Lang, M.; Paquet, E.; Neppel, L.; Sauquet, E. Changes in Mediterranean Flood Processes and Seasonality. *Hydrol. Earth Syst. Sci.* **2023**, *27*, 2973–2987. [CrossRef]
7. Tabari, H. Climate Change Impact on Flood and Extreme Precipitation Increases with Water Availability. *Sci. Rep.* **2020**, *10*, 13768. [CrossRef]
8. EEA. *Climate Change Impacts on Water Quality and Biodiversity Background Report for EEA European Environment*; ETC Water Technical Report 1/2010; EEA: Copenhagen, Denmark, 2010.
9. Sesana, E.; Gagnon, A.S.; Bonazza, A.; Hughes, J.J. An Integrated Approach for Assessing the Vulnerability of World Heritage Sites to Climate Change Impacts. *J. Cult. Herit.* **2020**, *41*, 211–224. [CrossRef]
10. Alfieri, L.; Bisselink, B.; Dottori, F.; Naumann, G.; de Roo, A.; Salamon, P.; Wyser, K.; Feyen, L. Global Projections of River Flood Risk in a Warmer World. *Earths Future* **2017**, *5*, 171–182. [CrossRef]
11. Vousdoukas, M.I.; Mentaschi, L.; Voukouvalas, E.; Verlaan, M.; Jevrejeva, S.; Jackson, L.P.; Feyen, L. Global Probabilistic Projections of Extreme Sea Levels Show Intensification of Coastal Flood Hazard. *Nat. Commun.* **2018**, *9*, 2360. [CrossRef]
12. Raymond, C.; Horton, R.M.; Zscheischler, J.; Martius, O.; AghaKouchak, A.; Balch, J.; Bowen, S.G.; Camargo, S.J.; Hess, J.; Kornhuber, K.; et al. Understanding and Managing Connected Extreme Events. *Nat. Clim. Chang.* **2020**, *10*, 611–621. [CrossRef]
13. Anghel, C.G.; Ilinca, C. Evaluation of Various Generalized Pareto Probability Distributions for Flood Frequency Analysis. *Water* **2023**, *15*, 1557. [CrossRef]
14. Ilinca, C.; Anghel, C.G. Flood-Frequency Analysis for Dams in Romania. *Water* **2022**, *14*, 2884. [CrossRef]
15. Peel, M.C.; Finlayson, B.L.; McMahon, T.A. Updated World Map of the Köppen-Geiger Climate Classification. *Hydrol. Earth Syst. Sci.* **2007**, *11*, 1633–1644. [CrossRef]
16. Zittis, G.; Bruggeman, A.; Camera, C.; Hadjinicolaou, P.; Lelieveld, J. The Added Value of Convection Permitting Simulations of Extreme Precipitation Events over the Eastern Mediterranean. *Atmos. Res.* **2017**, *191*, 20–33. [CrossRef]
17. Zachariadis, T. Forecast of Electricity Consumption in Cyprus up to the Year 2030: The Potential Impact of Climate Change. *Energy Policy* **2010**, *38*, 744–750. [CrossRef]
18. Rudari, R. *Words into Action Guidelines: National Disaster Risk Assessment Hazard Specific Risk Assessment 4*; Flood Hazard and Risk Assessment; UNDRR: Geneva, Switzerland, 2017.
19. Rincón, D.; Khan, U.T.; Armenakis, C. Flood Risk Mapping Using GIS and Multi-Criteria Analysis: A Greater Toronto Area Case Study. *Geosciences* **2018**, *8*, 275. [CrossRef]
20. Mudashiru, R.B.; Sabtu, N.; Abustan, I.; Balogun, W. Flood Hazard Mapping Methods: A Review. *J. Hydrol.* **2021**, *603*, 126846. [CrossRef]
21. Delipetrou, P.; Makhzoumi, J.; Dimopoulos, P.; Georghiou, K. Cyprus. In *Mediterranean Island Landscapes: Natural and Cultural Approaches*; Springer: Berlin/Heidelberg, Germany, 2008; pp. 170–203. [CrossRef]
22. WDD (TAY). 2nd_FRMP_CY001. WDD (TAY). 2023. Available online: https://www.moa.gov.cy/moa/wdd/wfdf.nsf/All/3119F26DD5476A96C2258A6E00413ECC/$file/2nd_FRMP_CY001.pdf?OpenElement (accessed on 31 July 2024).
23. Shustikova, I.; Domeneghetti, A.; Neal, J.C.; Bates, P.; Castellarin, A. Comparing 2D Capabilities of HEC-RAS and LISFLOOD-FP on Complex Topography. *Hydrol. Sci. J.* **2019**, *64*, 1769–1782. [CrossRef]
24. Mihu-Pintilie, A.; Cîmpianu, C.I.; Stoleriu, C.C.; Pérez, M.N.; Paveluc, L.E. Using High-Density LiDAR Data and 2D Streamflow Hydraulic Modeling to Improve Urban Flood Hazard Maps: A HEC-RAS Multi-Scenario Approach. *Water* **2019**, *11*, 1832. [CrossRef]
25. Patel, D.P.; Ramirez, J.A.; Srivastava, P.K.; Bray, M.; Han, D. Assessment of Flood Inundation Mapping of Surat City by Coupled 1D/2D Hydrodynamic Modeling: A Case Application of the New HEC-RAS 5. *Nat. Hazards* **2017**, *89*, 93–130. [CrossRef]
26. Papaioannou, G.; Efstratiadis, A.; Vasiliades, L.; Loukas, A.; Michael Papalexiou, S.; Koukouvinos, A.; Tsoukalas, I.; Kossieris, P. An Operational Method for Flood Directive Implementation in Ungauged Urban Areas. *Hydrology* **2018**, *5*, 24. [CrossRef]
27. Kim, H.I.; Keum, H.J.; Han, K.Y. Real-Time Urban Inundation Prediction Combining Hydraulic and Probabilistic Methods. *Water* **2019**, *11*, 293. [CrossRef]
28. Peña, F.; Nardi, F. Floodplain Terrain Analysis for Coarse Resolution 2D Flood Modeling. *Hydrology* **2018**, *5*, 52. [CrossRef]
29. Psomiadis, E.; Tomanis, L.; Kavvadias, A.; Soulis, K.X.; Charizopoulos, N.; Michas, S. Potential Dam Breach Analysis and Flood Wave Risk Assessment Using HEC-RAS and Remote Sensing Data: A Multicriteria Approach. *Water* **2021**, *13*, 364. [CrossRef]
30. Papaioannou, G.; Loukas, A.; Vasiliades, L.; Aronica, G.T. Flood Inundation Mapping Sensitivity to Riverine Spatial Resolution and Modelling Approach. *Nat. Hazards* **2016**, *83*, 117–132. [CrossRef]

31. Costabile, P.; Macchione, F. Enhancing River Model Set-up for 2-D Dynamic Flood Modelling. *Environ. Model. Softw.* **2015**, *67*, 89–107. [CrossRef]
32. Zittis, G.; Bruggeman, A.; Camera, C. 21st Century Projections of Extreme Precipitation Indicators for Cyprus. *Atmosphere* **2020**, *11*, 343. [CrossRef]
33. Wilson, J.P.; John, P.; Gallant, J.C. *Terrain Analysis: Principles and Applications*; Wiley: Hoboken, NJ, USA, 2000; ISBN 0471321885.
34. Hengl, T.; Reuter, H.I. *Geomorphometry-Concepts, Software, Applications*; Elsevier: Amsterdam, The Netherlands, 2009.
35. Ghostine, R.; Hoteit, I.; Vazquez, J.; Terfous, A.; Ghenaim, A.; Mose, R. Comparison between a Coupled 1D-2D Model and a Fully 2D Model for Supercritical Flow Simulation in Crossroads. *J. Hydraul. Res.* **2015**, *53*, 274–281. [CrossRef]
36. Ghostine, R.; Vazquez, J.; Terfous, A.; Mose, R.; Ghenaim, A. Comparative Study of 1D and 2D Flow Simulations at Open-Channel Junctions. *J. Hydraul. Res.* **2012**, *50*, 164–170. [CrossRef]
37. Brunner, G.W.; Piper, S.S.; Jensen, M.R.; Chacon, B. Combined 1D and 2D Hydraulic Modeling within HEC-RAS. In *World Environmental and Water Resources Congress 2015: Floods, Droughts, and Ecosystems—Proceedings of the 2015 World Environmental and Water Resources Congress, Austin, Texas, 17–21 May 2015*; ASCE: Reston, VA, USA, 2015; pp. 1432–1443. [CrossRef]
38. Henonin, J.; Russo, B.; Mark, O.; Gourbesville, P. Real-Time Urban Flood Forecasting and Modelling—A State of the Art. *J. Hydroinform.* **2013**, *15*, 717–736. [CrossRef]
39. Barreiro, J.; Santos, F.; Ferreira, F.; Neves, R.; Matos, J.S. Development of a 1D/2D Urban Flood Model Using the Open-Source Models SWMM and MOHID Land. *Sustainability* **2023**, *15*, 707. [CrossRef]
40. Dottori, F.; Salamon, P.; Bianchi, A.; Alfieri, L.; Hirpa, F.A.; Feyen, L. Development and Evaluation of a Framework for Global Flood Hazard Mapping. *Adv. Water Resour.* **2016**, *94*, 87–102. [CrossRef]
41. Quirogaa, V.M.; Kurea, S.; Udoa, K.; Manoa, A. Application of 2D Numerical Simulation for the Analysis of the February 2014 Bolivian Amazonia Flood: Application of the New HEC-RAS Version 5. *Ribagua* **2016**, *3*, 25–33. [CrossRef]
42. Md, M.; Yazdan, S.; Ahad, T.; Kumar, R.; Abdullah, M.; Mehedi, A. Estimating Flooding at River Spree Floodplain Using HEC-RAS Simulation. *J* **2022**, *5*, 410–426. [CrossRef]
43. Rangari, V.A.; Umamahesh, N.V.; Bhatt, C.M. Assessment of Inundation Risk in Urban Floods Using HEC RAS 2D. *Model. Earth Syst. Environ.* **2019**, *5*, 1839–1851. [CrossRef]
44. Costabile, P.; Costanzo, C.; Ferraro, D.; Macchione, F.; Petaccia, G. Performances of the New HEC-RAS Version 5 for 2-D Hydrodynamic-Based Rainfall-Runoff Simulations at Basin Scale: Comparison with a State-of-the Art Model. *Water* **2020**, *12*, 2326. [CrossRef]
45. Samarasinghe, J.T.; Basnayaka, V.; Gunathilake, M.B.; Azamathulla, H.M.; Rathnayake, U. Comparing Combined 1D/2D and 2D Hydraulic Simulations Using High-Resolution Topographic Data: Examples from Sri Lanka—Lower Kelani River Basin. *Hydrology* **2022**, *9*, 39. [CrossRef]

Disclaimer/Publisher's Note: The statements, opinions and data contained in all publications are solely those of the individual author(s) and contributor(s) and not of MDPI and/or the editor(s). MDPI and/or the editor(s) disclaim responsibility for any injury to people or property resulting from any ideas, methods, instructions or products referred to in the content.